

Article

A Sub-Threshold Differential CMOS Schmitt Trigger with Adjustable Hysteresis Based on Body Bias Technique

Sara Radfar ¹, Ali Nejati ¹, Yasin Bastan ¹ , Parviz Amiri ^{1,*}, Mohammad Hossein Maghami ¹ , Mehdi Nasrollahpour ² and Sotoudeh Hamed-Hagh ^{2,*}

¹ Microelectronics and Industrial Equipment Laboratory, Department of Electrical Engineering, Shahid Rajaee Teacher Training University, 1678815811 Tehran, Iran; s.radfar@sru.ac.ir (S.R.); ali.nejati.srtt@gmail.com (A.N.); ybastan@srttu.edu (Y.B.); mhmaghami@sru.ac.ir (M.H.M.)

² Department of Electrical Engineering, San Jose State University, San Jose, CA 95192, USA; nasrollahpourmotla.m@husky.neu.edu

* Correspondence: pamiri@sru.ac.ir (P.A.); sotoudeh.hamed-hagh@sjsu.edu (S.H.-H.)

Received: 8 April 2020; Accepted: 10 May 2020; Published: 14 May 2020



Abstract: This paper presents a sub-threshold differential CMOS Schmitt trigger with tunable hysteresis, which can be used to enhance the noise immunity of low-power electronic systems. By exploiting the body bias technique to the positive feedback transistors, the hysteresis of the proposed Schmitt trigger is generated, and it can be adjusted by the applied bias voltage to the bulk terminal of the utilized PMOS transistors. The principle of operation and the main formulas of the proposed circuit are discussed. The circuit is designed in a 0.18- μm standard CMOS process with a 0.6 V power supply. Post-layout simulation results show that the hysteresis width of the Schmitt trigger can be adjusted from 45.5 mV to 162 mV where the ratio of the hysteresis width variation to supply voltage is 19.4%. This circuit consumes $10.52 \times 7.91 \mu\text{m}^2$ of silicon area, and its power consumption is only 1.38 μW , which makes it a suitable candidate for low-power applications such as portable electronic, biomedical, and bio-implantable systems.

Keywords: differential Schmitt trigger; low voltage; sub-threshold; low power; body bias technique; positive feedback

1. Introduction

As the electronics world is heading toward the future, electronic devices require longer lifetime batteries. Hence, the IC designers are obliged to make use of some design techniques to provide a prolonged battery life. One of the common techniques is reducing the supply voltage to decrease the power consumption of the circuits by operating transistors in the weak inversion region. At low voltage, one of the main constraints faced is the device noise level. The weak inversion region is also known as the sub-threshold region because it occurs under the threshold voltage of transistors where very small currents can be provided. The current-voltage equation in this region is an exponential relationship, and although for a given power budget, the g_m/I_D ratio is at its maximum level; since the values of currents are so small, the circuit may become sensitive to noise [1,2]. Moreover, circuits which operate in the sub-threshold region face some limitations such as poor frequency response and poor linearity [2]. Thus, in general, these circuits are meant for low-frequency and low-current applications such as biomedical and biotelemetry devices and are not suitable for medium power applications [3,4].

A valuable solution to improve the robustness of the circuits to noise is using Schmitt triggers. Schmitt triggers can improve the sensitivity of electronic systems to electromagnetic interferences, i.e., they increase the static noise margin of the circuits but at the cost of more power consumption

and delay [5,6]. Accordingly, in general, it is expected that the circuits based on Schmitt triggers operate more reliably in terms of noise immunity [7]. The Schmitt trigger is a bi-stable circuit that is utilized in both analog and digital signal processing systems [8]. The reason for the popularity of this circuit is its hysteresis characteristic or its ability to work in two different threshold levels, which enables the Schmitt trigger to suppress noise in various analog and digital circuits [9]. Indeed, the Schmitt trigger is a restoring signal circuit [10], which eliminates noise content from the input signal and extracts the original input signal information. The positive feedback that causes the circuit loop gain to be more than one is the most popular scheme in creating distinct threshold levels to provide the hysteresis characteristic. The feature that equips the Schmitt trigger with analog to digital conversion and therefore reshapes the pulses can be implemented by either internal or external positive feedback. The positive feedback can be controlled internally or externally according to the intended application and noise tolerance [11,12]. It is worth noting that since different threshold levels can cause different outputs, the hysteresis characteristic might not be desirable in some applications, such as ADC converters [13].

Hysteresis of a Schmitt trigger is directly affected by process variations and transistor mismatches. This issue is more problematic in applications where the level of noise and disturbances is not predictable [8]. To overcome this deficiency, Schmitt triggers with tunable hysteresis can be used as a helpful solution. Besides, the possibility of controlling the hysteresis levels in some applications such as power amplifier circuits [14] leads to lower power consumption and improves the overall performance of the circuit [15].

Generally, traditional single-output Schmitt triggers used to be realized by operational amplifiers and passive components, which had some significant defects such as high-power consumption, limited-gain bandwidth product, low-slew rate, and low-dynamic range. After Allstot, who designed a Schmitt trigger for wireless applications [16], implementing differential Schmitt triggers became widely common. Nowadays, Schmitt triggers, which can convert any periodic signal to its stable logic one, are the fundamental block frequently used in the areas of communication and measurement systems to generate basic waveforms such as square, triangular, pulse, and so on [17–19]. Furthermore, relaxation oscillators [20], function generators [21], mono-stable multi-vibrators [22], pulse width modulators [23], and switching power supplies [24] are the other several applications of Schmitt trigger circuits in the emerging areas of signal processing.

In this paper, a differential Schmitt trigger with adjustable hysteresis and transistors that are biased in the sub-threshold region is proposed. Hysteresis of this circuit is created by positive feedback and can be controlled by the body bias technique. In a body driven transistor, the input signal is applied to the bulk terminal to create conduction between the source and drain. Despite the smaller transconductance and bandwidth, this will enhance the application of fundamental analog building blocks in low-voltage environments [2]. In the presented work, by applying the body bias technique to the positive feedback transistors, no additional element is required to equip the circuit with hysteresis control capability. Basically, MOSFETs using the body bias technique are required to have isolated bulk terminals [2], which cause some percent of a larger active area. However, the proposed circuit structure helps to have a Schmitt trigger with fewer transistors and a smaller occupied chip area compared to the recently proposed topologies, which make it suitable for bio-implantable circuits. This paper is organized as follows: The proposed Schmitt trigger is described in Section 2; Section 3 presents the simulation results; finally, the paper is concluded in Section 4.

2. Proposed Schmitt Trigger Circuit Description

2.1. Differential Pair of the Circuit

The differential pair of the proposed low-voltage, low-power Schmitt trigger with tunable hysteresis is illustrated in Figure 1. Transistors of M_{1a} and M_{1b} are the differential inputs, and M_t is a controlled current source that provides the tail current of the differential pair by a bias voltage of V_{B1} . M_{2a} and M_{2b} implement positive feedback to create the hysteresis of the proposed Schmitt trigger.

Due to the tail current, when the DC voltage of the positive input, V_{in}^+ , increases from 0 to positive voltages while V_{in}^- is fixed at a mid-point (reference voltage), I_{1a} will be increased, and inversely, I_{1b} will be decreased, which are the drain currents of transistors M_{1a} and M_{1b} , respectively. Thus, based on the differential behavior of the circuit, the drain voltage of M_{1a} decreases and the drain voltage of M_{1b} increases, and V_{d-1a} switches from high to low in V_2 . The DC transfer characteristics of V_{d-1a} are shown in Figure 2 (gray curve).

It should be noted that because of M_{3a} , which is a voltage-controlled current source and provides a fixed current, an increase in I_{1a} will increase the drain current of M_{2a} , i.e., I_{2a} . On the other hand, when I_{1b} decreases, I_{2b} reduces as well under the same circumstance. However, the reduction of V_{d-1a} will force I_{2b} to increase and retain its former situation. Therefore, I_{1b} and accordingly V_{d-1b} will not change either. Hence, I_{2a} will also retain its former situation, and I_{1a} and V_{d-1a} will remain unchanged as well. This situation will continue until the difference between V_{in}^+ and V_{in}^- becomes so large that I_{1a} overcomes I_{2a} and the state changes. At this point, V_{d-1a} will change; its position is denoted as V_3 in Figure 2. In contrast, when V_{in}^+ becomes significantly smaller than V_{in}^- , the output current will change its state at the voltage of V_1 , which is shown in the figure. This voltage shift from V_2 is caused by the positive feedback transistors; M_{2a} and M_{2b} . In the absence of these transistors, the circuit will operate as a comparator. It is perceivable that the proposed Schmitt trigger operates at a current mode, and its operation analysis is described in the following.

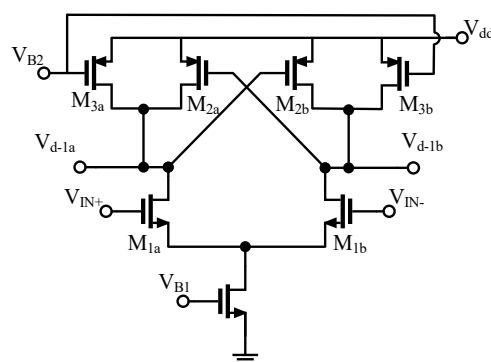


Figure 1. The differential pair of the proposed Schmitt trigger.

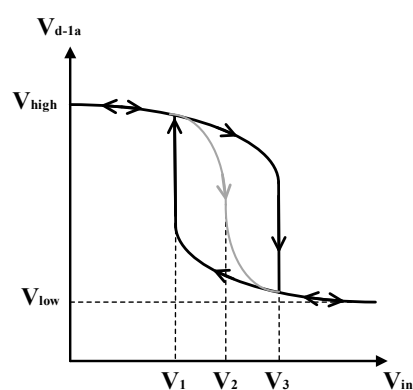


Figure 2. Qualitative hysteresis characteristic of an inverting Schmitt trigger.

According to Figure 1, using KCL at the drain node of the positive input transistor M_{1a} results in:

$$I_{1a} = I_{3a} + I_{2a}, \quad (1)$$

The drain current equation in the sub-threshold region has an exponential relationship and for a NMOS transistor equals to $I_d = I_0 \frac{W}{L} e^{\frac{V_{gs}}{nV_t}} (1 - e^{-\frac{V_{ds}}{V_t}})$ where $I_0 = \mu_n C_{ox} (n-1) V_t^2 e^{-\frac{V_{th}}{nV_t}}$. Then, I_d can be

approximated as $I_d = I_0 \frac{W}{L} e^{\frac{V_{gs} - V_{th}}{nV_t}}$ where n and V_t are sub-threshold coefficient and thermal voltage, respectively. Consequently, Equation (1) can be written as:

$$I_{0,1a} \left(\frac{W}{L} \right)_{1a} e^{\frac{V_{gs,1a} - V_{th,1a}}{nV_t}} = I_{3a} + I_{0,2a} \left(\frac{W}{L} \right)_{2a} e^{\frac{|V_{gs,2a}| - |V_{th,2a}|}{nV_t}}, \quad (2)$$

If we repeat the same path for the drain node of the negative input transistor M_{1b} and subtract $V_{gs,1b}$ from $V_{gs,1a}$, the voltage difference of input terminals becomes:

$$\Delta V_{in} = (V_{gs,2a} - V_{gs,2b}) + (V_{th,2b} - V_{th,2a}), \quad (3)$$

2.2. Two-Stage Schmitt Trigger Circuit

In Figure 2, voltage levels of V_1 and V_3 are LTP and UTP of the Schmitt trigger, respectively. As can be seen, the hysteresis curve will not reach to logical zero or one, which is because of the low gain of the circuit. To solve this problem, an output stage is added to the structure illustrated in Figure 3. After amplifying the signal by the second stage, the hysteresis characteristic will be consistent with Figure 4. In other words, immediately after V_{d-1a} 's decrease, the drain current of M_{4a} will also reduce. Then, because of the current mirror of $M_{5a,b}$ and higher current of M_{4b} , I_{out} will approach zero and a sharper transition will occur, as depicted in Figure 4.

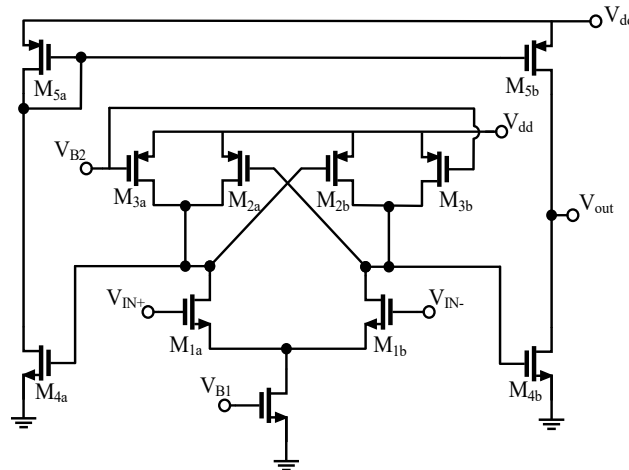


Figure 3. The proposed two-stage Schmitt trigger.

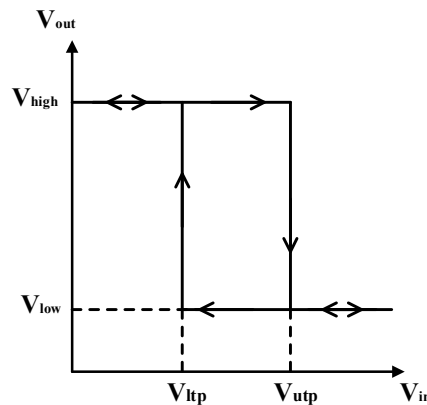


Figure 4. Qualitative hysteresis characteristic of the two-stage Schmitt trigger.

A KVL from V_{dd} to the source terminal of M_{4b} will result in $V_{gs,2a} = -V_{dd} + V_{gs,4b}$. Afterward, we can write:

3. Post-Layout Simulation Results

The proposed sub-threshold differential Schmitt trigger with tunable hysteresis is designed and post-layout simulated in a standard 0.18 μm CMOS technology. The utilized technology allows bulk and body contacts to be different in the wafer fabrication process. Power consumption of the circuit is 1.38 μW , which makes it suitable for biomedical applications. The layout of the proposed Schmitt trigger is shown in Figure 6, which occupies the chip area of $10.52 \times 7.91 \mu\text{m}^2$. The aspect ratios of transistors are set according to Table 1.

Table 1. Aspect ratios of the transistors.

Transistor	W/L
$M_{1a,b}$	0.44 $\mu\text{m}/0.18 \mu\text{m}$
$M_{2a,b}$	0.88 $\mu\text{m}/0.18 \mu\text{m}$
$M_{3a,b}$	0.44 $\mu\text{m}/0.18 \mu\text{m}$
$M_{4a,b}$	0.44 $\mu\text{m}/0.18 \mu\text{m}$
$M_{5a,b}$	0.88 $\mu\text{m}/0.18 \mu\text{m}$
M_t	0.44 $\mu\text{m}/0.18 \mu\text{m}$

The DC voltage transfer characteristic of the proposed Schmitt trigger is shown in Figure 7 where V_{in}^+ is initially swept from 0 to 0.6 V and then from 0.6 V to 0 to observe the hysteresis curve, while V_{in}^- is fixed at 0.3 V. The UTP and LTP of the circuit are 380.1 mV and 254.1 mV, respectively, so the hysteresis width is 126 mV. A triangular waveform with the amplitude of 0.6 V and 500 kHz frequency is applied to V_{in}^+ , and its corresponding transient output is illustrated in Figure 8.

Figure 9 shows the hysteresis characteristic of the proposed Schmitt trigger while V_{c1} is swept from 0.3 V to 0.6 V. It is clear that the hysteresis width can be varied in proportion to the bias voltage applied to the bulk terminal of the positive feedback transistors M_{2a} and M_{2b} . Moreover, the variation of the transient response of the circuit according to the changes of the body bias voltage, i.e., V_{c1} , is depicted in Figure 10. The voltage transfer characteristic of the proposed Schmitt trigger over different process corners at 27 $^{\circ}\text{C}$ is shown in Figure 11. Variations of the hysteresis width and the center of the circuit in three process corners over temperatures from -20°C to 60°C is simulated, and the result is illustrated in Figure 12a,b, respectively.

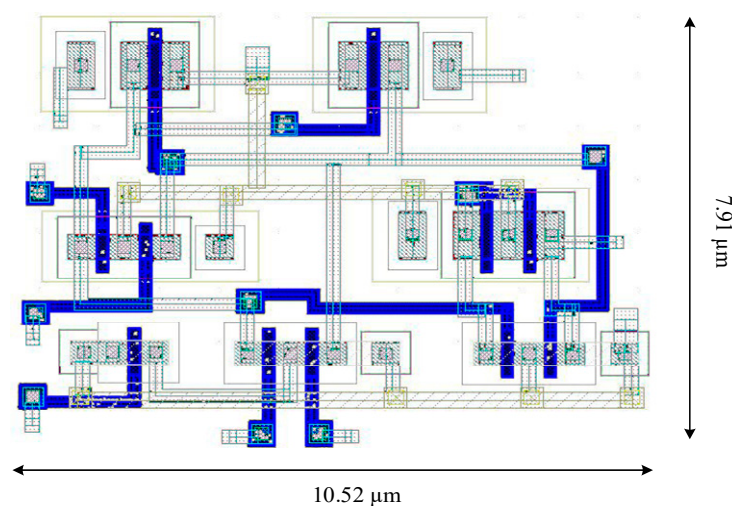


Figure 6. The layout of the proposed Schmitt trigger in 0.18 μm CMOS technology.

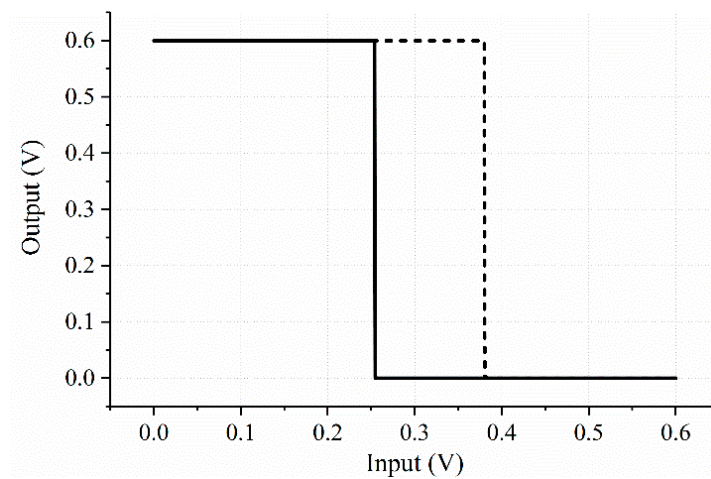


Figure 7. Voltage transfer characteristics of the proposed Schmitt trigger. V_{in}^+ is swept from 0 to 0.6 V and vice versa, while V_{in}^- is set to 0.3 V, and V_{B1} and V_{B2} are 0.35 V and 0.3 V, respectively.

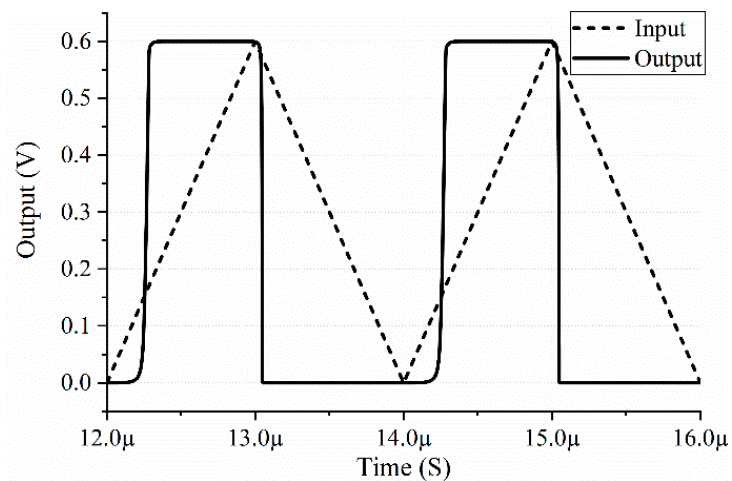


Figure 8. Time-domain response of the designed Schmitt trigger circuit to 500 kHz triangular input signal.

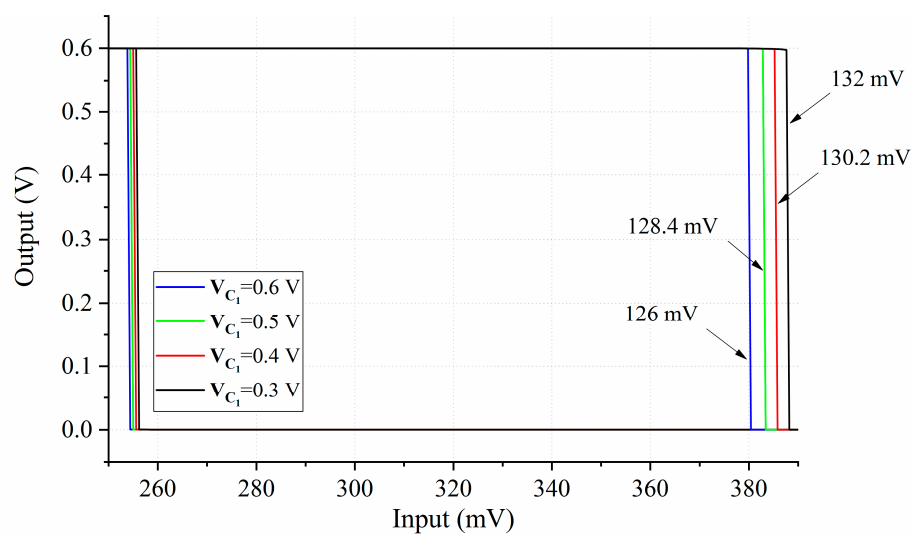


Figure 9. Dependence of the threshold voltages on the V_{c1} variation. V_{in}^+ is swept from 0 to 0.6 V and vice versa, while V_{in}^- is set to 0.3 V.

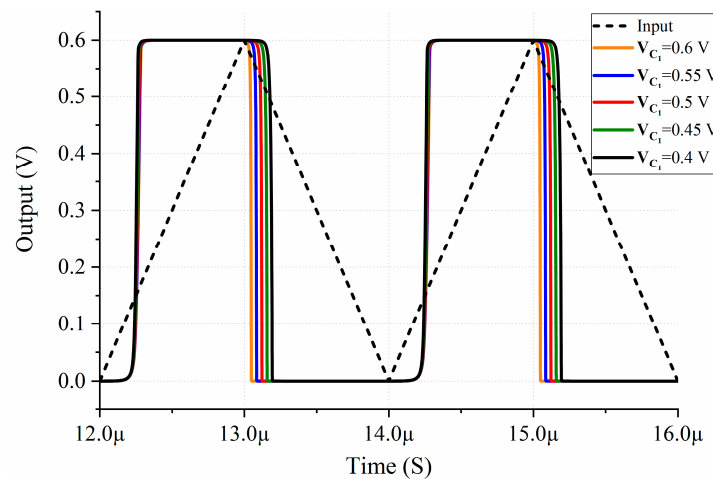


Figure 10. Variation of the time-domain response of the proposed circuit by changes of V_{C1} .

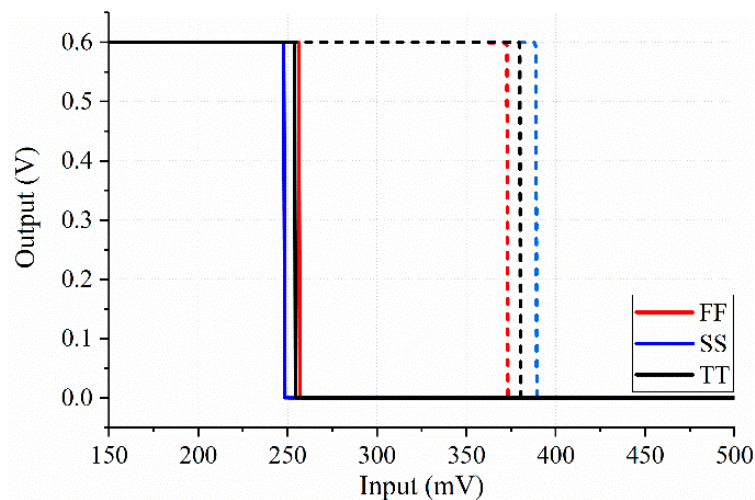


Figure 11. Variation of the hysteresis width in different process corners at 27 degrees Celsius.

Figure 13 shows the variation of the hysteresis width and its center versus the reference voltage for a constant value of control voltage. In addition to the hysteresis width variation of the circuit by changing V_{C1} , the width and the center of its hysteresis vary through sweeping V_{in-} from 250 mV to 450 mV. Figure 14 provides a more comprehensive review of the dependency of the hysteresis width on the control voltage and the reference voltage. It shows that by sweeping V_{C1} from 400 mV to 600 mV and simultaneously changing V_{in-} from 250 mV to 350 mV, hysteresis width changes in a range of 116 mV.

To examine the effect of process variations and component mismatches on the transient response of the proposed Schmitt trigger, 100 runs of Monte Carlo analysis are performed for all employed transistors. Figure 15 shows the transient responses of input and output voltages for post-layout simulation of Monte Carlo analysis. Finally, in Figure 16a,b, post-layout simulated histograms for 100 runs of Monte Carlo for LTP and UTP of the circuit are presented. As can be seen, the majority of the iterations for LTP and UTP fit in about $254 \text{ mV} \pm 11\%$ and $380 \text{ mV} \pm 15\%$, respectively. Moreover, the proposed circuit was simulated with $\pm 10\%$ variation in power supply, for which proper operation was observed (Figure 17).

Table 2 illustrates the comparison of the proposed and the recent CMOS Schmitt triggers which have almost common properties. The comparison is mainly considered in terms of supply voltage, single or differential input, voltage or current mode, static power consumption, occupied chip area, and hysteresis width. The proposed current mode CMOS Schmitt trigger operates at a voltage supply

of 0.6 V and its transistors are biased in the sub-threshold region. Therefore, this circuit has significantly lower power consumption and a smaller occupied chip area, which make it suitable for low-voltage and low-power applications.

Table 2. Performance comparison of Schmitt triggers.

	This Work	[15]	[25]	[26]	[27]	[28]	[29]	[30]
Technology	0.18 μm CMOS	0.18 μm CMOS	0.18 μm CMOS	0.18 μm CMOS	0.18 μm CMOS	0.18 μm CMOS	40 nm CMOS	0.18 μm CMOS
Power Supply	0.6 V	1.8 V	0.8 V	0.6 V	0.4 V	0.15 V	1 V	0.4 V
Single/Differential Input	Diff.	Diff.	Diff.	Single	Diff.	Single	Single	Pseudo Diff.
V/I Mode	Current Mode (I)	Current Mode (I)	Current Mode (I)	Voltage Mode (V)	Current Mode (I)	Current Mode (I)	Voltage Mode (V)	Current Mode (I)
Variable/Fixed Hysteresis	Variable	Variable	Variable	Fixed	Fixed	Fixed	Variable	Fixed
$\frac{W_H}{V_{DD}}^1$	19.4%	6.66%	12.5%	0	0	0	2.8%	0
Power Consumption	1.38 μW	-	0.48–1.12 mW	2.64 mW	-	-	-	150 nW
Chip Area	(10.52 \times 7.91) μm^2	-	(39 \times 17.5) μm^2	-	-	(20.37 \times 10.41) μm^2	-	(14.8 \times 7) μm^2
No. of Transistors	11 + bias	13	16 + bias	9	14 + bias	6	6	10 + bias
Simulation/Measurement	Post-layout Sim.	Sim.	Post-layout Sim.	Meas.	Sim.	Meas.	Sim.	Post-layout Sim.

¹ W_H : Hysteresis width variation.

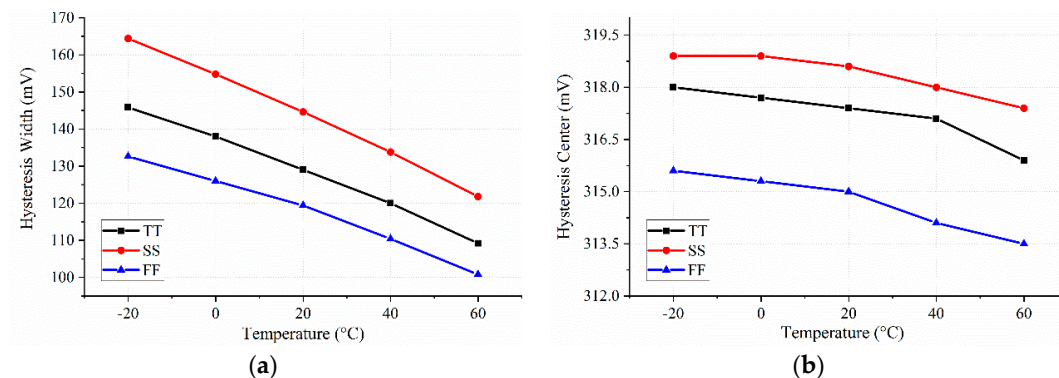


Figure 12. Variation of hysteresis (a) width and (b) center of the proposed Schmitt trigger from -20 to 60 degrees Celsius in different process corners.

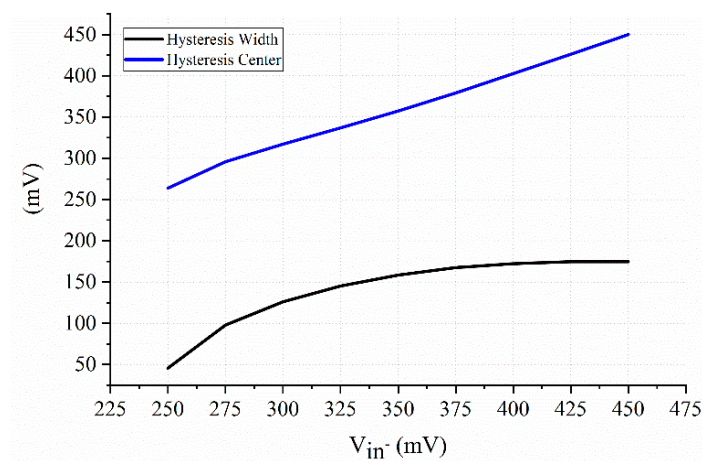


Figure 13. Variation of the hysteresis width and its center versus reference voltage of V_{in-} while V_{C1} is set to 300 mV.

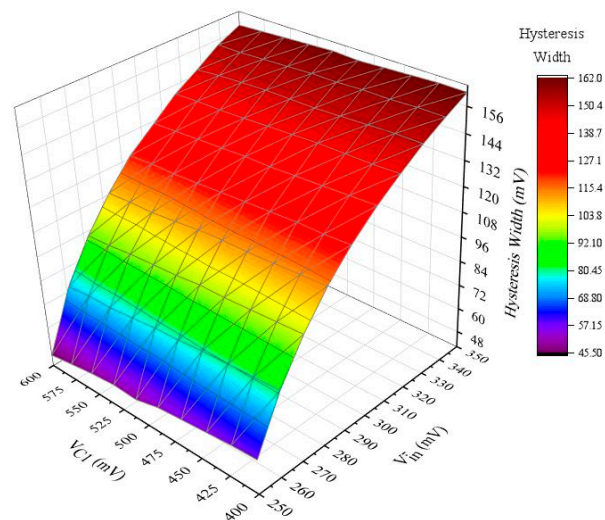


Figure 14. Dependence of the hysteresis width on the control voltage (V_{C1}) and the reference voltage (V_{in-}).

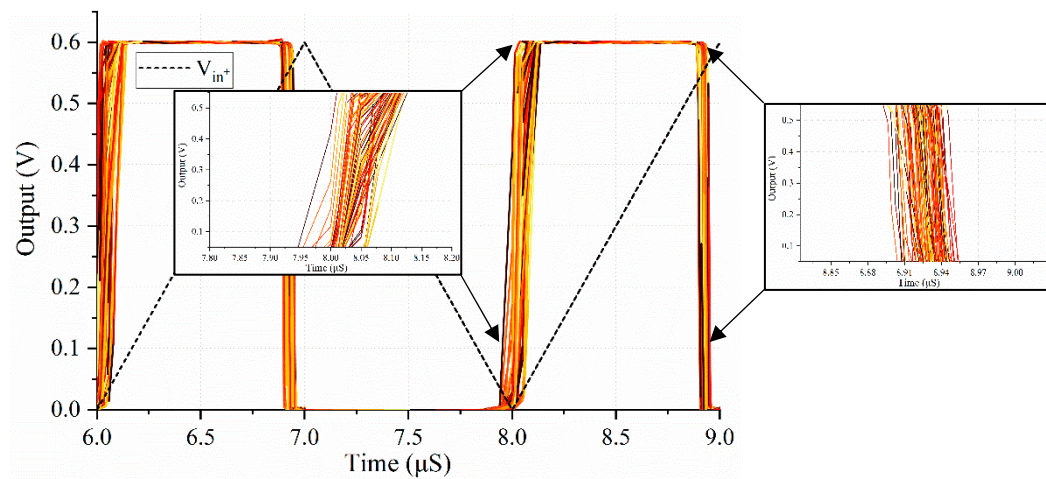


Figure 15. Post-layout simulation for 100 runs of Monte Carlo on the transient response of the input and output voltages.

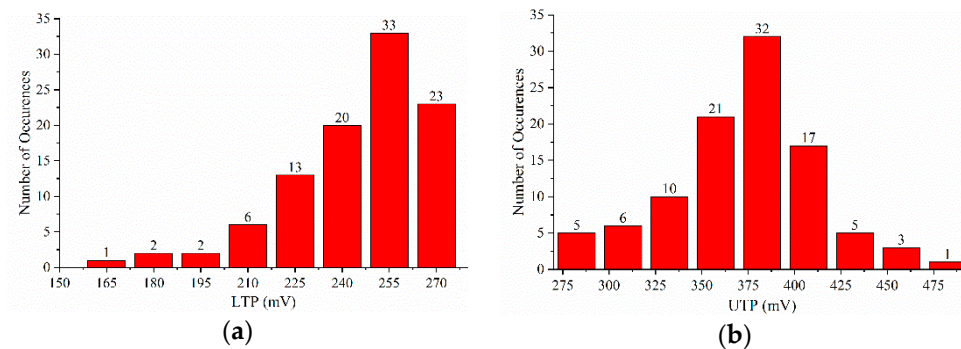


Figure 16. Post-layout simulated histogram for 100 runs of Monte Carlo for (a) LTP and (b) UTP.

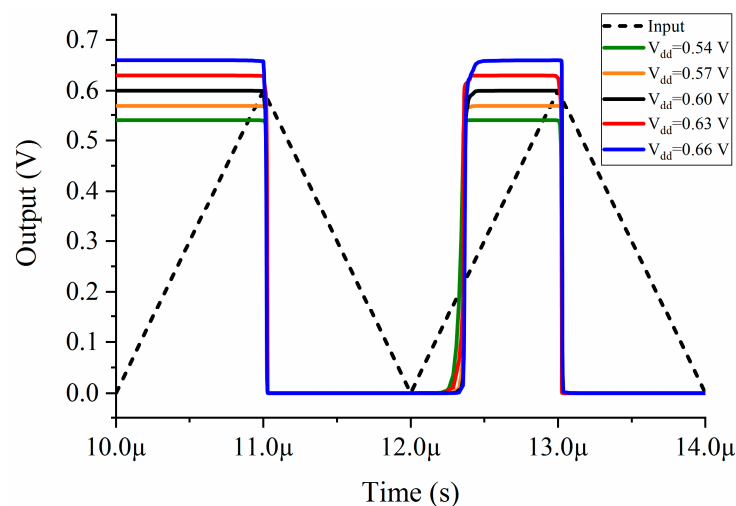


Figure 17. Transient response of the output voltage with $\pm 10\%$ on the power supply for a triangular saw-tooth input voltage.

4. Conclusions

A low-voltage, low-power differential Schmitt trigger for biomedical applications, which operates at 0.6 V supply voltage and current mode, has been presented in this paper. By applying bias voltages in the range of 0.3 V to 0.6 V to the positive feedback transistors, the hysteresis width of the proposed circuit can be varied from 126 mV to 132 mV, which means that its hysteresis width is adjusted by the body bias technique. Moreover, by changing the control voltage and reference voltage simultaneously, a bigger range of hysteresis width variation from 45.5 mV to 162 mV is achievable. This Schmitt trigger consumes 1.38 μW of static power and occupies $10.52 \times 7.91 \mu\text{m}^2$ of the chip area. Properties of this circuit make it a good candidate for low-voltage and low-power applications such as electronic healthcare devices and implantable microsystems.

Author Contributions: Conceptualization and design, S.R. and A.N.; formal analysis, A.N. and S.R.; software, A.N. and S.R.; investigation, M.H.M. and Y.B.; writing—original draft preparation, S.R.; writing—review and editing, M.N. and S.H.-H.; supervision, P.A. and M.H.M.; funding acquisition, S.H.-H. and M.N. All authors have read and agreed to the published version of the manuscript.

Funding: This research received no external funding.

Conflicts of Interest: The authors declare no conflict of interest.

References

1. Sansen, W. *Analog Design Essentials*; Springer: Dordrecht, The Netherlands, 2006.
2. Rajput, S.; Jamuar, S. Low Voltage Analog Circuit Design Techniques. *IEEE Circuits Syst. Mag.* **2002**, *2*, 24–42. [\[CrossRef\]](#)
3. Calhoun, B.; Chandrakasan, A. A 256-Kb 65-Nm Sub-Threshold SRAM Design for Ultra-Low-Voltage Operation. *IEEE J. Solid-State Circuits* **2007**, *42*, 680–688. [\[CrossRef\]](#)
4. Lee, H.; Mohammadi, S. A 3GHz Subthreshold CMOS Low Noise Amplifier. In Proceedings of the IEEE Radio Frequency Integrated Circuits (RFIC) Symposium, San Francisco, CA, USA, 10–13 June 2006.
5. Kulkarni, J.; Roy, K. Ultralow-Voltage Process-Variation-Tolerant Schmitt-Trigger-Based SRAM Design. *IEEE Trans. on Very Large Scale Integr. (VLSI) Syst.* **2012**, *20*, 319–332. [\[CrossRef\]](#)
6. Lotze, N.; Manoli, Y. A 62 mV 0.13 μm CMOS Standard-Cell-Based Design Technique Using Schmitt-Trigger Logic. *IEEE J. Solid-State Circuits* **2012**, *47*, 47–60. [\[CrossRef\]](#)
7. Tache, M.; Ibrahim, W.; Kharbash, F.; Beiu, V. Reliability and Performance of Optimised Schmitt Trigger Gates. *J. Eng.* **2018**, *2018*, 735–744. [\[CrossRef\]](#)
8. Yuan, F. Differential CMOS Schmitt Trigger with Tunable Hysteresis. *Analog Integr. Circuits Signal Process.* **2009**, *62*, 245–248. [\[CrossRef\]](#)

9. Hagiwara, T.; Yamaguchi, K.; Shojiro, A. Threshold voltage deviation in very small MOS transistors due to local impurity fluctuations. In Proceedings of the 1982 Symposium on VLSI Technology. Digest of Technical Papers, Oiso, Japan, 1–3 September 1982; pp. 46–47.
10. Saxena, A.; Akashe, S. Comparative Analysis of Schmitt Trigger with AVL (AVLG and AVLS) Technique Using Nanoscale CMOS Technology. In Proceedings of the Third International Conference on Advanced Computing and Communication Technologies (ACCT), Rohtak, India, 6–7 April 2013.
11. Nandhasri, K.; Ngarmnil, J. Hysteresis tunable FG MOS comparator. In Proceedings of the ICSE 2000, 2000 IEEE International Conference on Semiconductor Electronics. Proceedings (Cat. No.00EX425), Guoman Port Dickson Resort, Malaysia, 13–15 November 2000.
12. Ekekwe, N.; Etienne-Cummings, R. Adaptive Hysteretic Comparator with Op-amp Threshold Level Setting. In Proceedings of the 51st Midwest Symposium on Circuits and Systems, Knoxville, TN, USA, 10–13 August 2008.
13. Goll, B.; Zimmermann, H. *Comparators in Nanometer CMOS Technology*; Springer: Berlin, Germany, 2016.
14. Amiri, P.; Nabavi, A.; Mortazavi, S. Low Distortion CMOS Class-D Amplifier with Double-Band Hysteresis. *IEICE Electron. Express* **2010**, *7*, 273–280. [[CrossRef](#)]
15. Yuan, F. A High-Speed Differential CMOS Schmitt Trigger with Regenerative Current Feedback and Adjustable Hysteresis. *Analog Integr. Circuits Signal Process.* **2009**, *63*, 121–127. [[CrossRef](#)]
16. Allstot, D. A Precision Variable-Supply CMOS Comparator. *IEEE J. Solid-State Circuits* **1982**, *17*, 1080–1087. [[CrossRef](#)]
17. Minaei, S.; Yuce, E. A Simple Schmitt Trigger Circuit with Grounded Passive Elements and Its Application to Square/Triangular Wave Generator. *Circuits Syst. Signal Process.* **2011**, *31*, 877–888. [[CrossRef](#)]
18. Kumar, A.; Chaturvedi, B. Single Active Element-Based Tunable Square/Triangular Wave Generator with Grounded Passive Components. *Circuitssyst. Signal Process.* **2017**, *36*, 3875–3900. [[CrossRef](#)]
19. Chung, W.; Kim, H.; Cha, H.; Kim, H. Triangular/Square-Wave Generator with Independently Controllable Frequency and Amplitude. *IEEE Trans. Instrum. Meas.* **2005**, *54*, 105–109. [[CrossRef](#)]
20. Onomi, T. Experimental Demonstration and Performance Estimation of a New Relaxation Oscillator Using a Superconducting Schmitt Trigger Inverter. *Phys. Procedia* **2016**, *81*, 141–144. [[CrossRef](#)]
21. Kumar, D.; Khatri, R. Function Generator Using Current Conveyor (CCII). *Int. J. Comput. Appl.* **2016**, *147*, 1–4. [[CrossRef](#)]
22. Chien, H.-C.; Lo, Y.-K. Design and Implementation of Monostable Multivibrators Employing Differential Voltage Current Conveyors. *Microelectron. J.* **2011**, *42*, 1107–1115. [[CrossRef](#)]
23. Lin, B. Phase-Shift PWM Converter with Wide Voltage Operation Capability. *Electronics* **2019**, *9*, 47. [[CrossRef](#)]
24. Newsom, R.; Dillard, W.; Nelms, R. Digital Power-Factor Correction for a Capacitor-Charging Power Supply. *IEEE Trans. Ind. Electron.* **2002**, *49*, 1146–1153. [[CrossRef](#)]
25. Nejati, A.; Bastan, Y.; Amiri, P.; Maghami, M. A Low-Voltage Bulk-Driven Differential CMOS Schmitt Trigger with Tunable Hysteresis. *J. Circuitssystems Comput.* **2019**, *28*, 1–14. [[CrossRef](#)]
26. Park, S.; Kim, K.; Huynh, H.A.; Joo, S.; Kim, S. EM Noise Immunity Enhancement Using Schmitt Trigger Logic Gates in CMOS Process. In Proceedings of the URSI Asia-Pacific Radio Science Conference (URSI AP-RASC), Seoul, Korea, 21–25 August 2016.
27. Nejati, A.; Bastan, Y.; Amiri, P. 0.4 V Ultra-Low Voltage Differential CMOS Schmitt Trigger. In Proceedings of the Iranian Conference on Electrical Engineering (ICEE), Tehran, Iran, 2–4 May 2017.
28. Melek, L.A.P.; Silva, A.L.D.; Schneider, M.C.; Galup-Montoro, C. Analysis and Design of the Classical CMOS Schmitt Trigger in Subthreshold Operation. *IEEE Trans. Circuits Syst. I Regul. Pap.* **2017**, *64*, 869–878. [[CrossRef](#)]
29. Chen, Z.; Chen, S. A High-Speed Low Voltage CMOS Schmitt Trigger with Adjustable Hysteresis. In Proceedings of the IEEE/ACIS 16th International Conference on Computer and Information Science (ICIS), Wuhan, China, 24–26 May 2017.
30. Bastan, Y.; Nejati, A.; Radfar, S.; Amiri, P.; Nasrollahpour, M.; Hamed-Hagh, S. An Ultra-Low-Voltage Sub-Threshold Pseudo-Differential CMOS Schmitt Trigger. In Proceedings of the 31st IEEE International System-on-Chip Conference (SOCC), Arlington, VA, USA, 4–7 September 2018.

